Converting Long-Range Entanglement into Mixture: Tensor-Network Approach to Local Equilibration

Miguel Frías-Pérez,[1,2,*] Luca Tagliacozzo,[3] and Mari Carmen Bañuls[1,2]
[1]Max-Planck-Institut für Quantenoptik, Hans-Kopfermann-Str. 1, D-85748 Garching, Germany
[2]Munich Center for Quantum Science and Technology (MCQST), Schellingstr. 4, D-80799 München, Germany
[3]Institute of Fundamental Physics IFF-CSIC, Calle Serrano 113b, 28006 Madrid, Spain

(Received 18 September 2023; accepted 30 January 2024; published 7 March 2024)

In the out-of-equilibrium evolution induced by a quench, fast degrees of freedom generate long-range entanglement that is hard to encode with standard tensor networks. However, local observables only sense such long-range correlations through their contribution to the reduced local state as a mixture. We present a tensor network method that identifies such long-range entanglement and efficiently transforms it into mixture, much easier to represent. In this way, we obtain an effective description of the time-evolved state as a density matrix that captures the long-time behavior of local operators with finite computational resources.

DOI: 10.1103/PhysRevLett.132.100402

Reconciling the time-reversal invariant unitary evolution of closed quantum many-body systems with the emergence of statistical mechanics and its well defined arrow of time is still an open question, hindered by the exponential complexity of simulating this problem in the generic case.

In contrast, the equilibrium wave functions of a large class of physically relevant systems live in a small corner of the exponentially large Hilbert space, characterized by a bounded amount of entanglement [1]. States therein admit an efficient approximation as a tensor network (TN) [2]. This property implies we can perform very precise numerical simulations with only polynomial resources [3–9], such as those with matrix product states (MPS) in one dimension [4,10–13].

Out of equilibrium, instead, initially localized correlations can propagate over arbitrarily large distances. As a result, the entanglement in the system increases rapidly [14–19] and simple TN Ansätze like MPS have limited applicability. By focusing on the local description of the state, nevertheless, one can circumvent the exponential complexity that originated from such nonlocal correlations. Significant simplifications using this approach have already been observed [20–30].

Here we develop this idea and propose a new algorithm that explicitly identifies long-range entanglement in the system and trades it for mixture (see also [26]). In particular, our method focuses on separating fast and slow propagating degrees of freedom. Already from an early time we observe that the fast degrees of freedom mediate nonlocal correlations whose effect on local observables is that of a statistical mixture. Using that knowledge, we devise a TN algorithm that provides an effective description of the time-evolved state as a density matrix, represented by a matrix product operator (MPO) with bounded bond dimension, and accurately captures the long-time behavior of local operators.

To benchmark the algorithm, we simulate quenches in the transverse field Ising model and its nonintegrable generalization. We find that our results agree with those dictated by, respectively, the analytical solutions and the prediction of the diagonal ensemble [31–33].

Quenches and quasiparticles.—We focus on quantum quenches [14,34], in which a one-dimensional system in the thermodynamic limit is prepared at $t = 0$ in a product state $|\psi_0\rangle$, and later evolved with an entangling Hamiltonian H. Our aim is to compute the time-dependent expectation value of a local observable O.

The initial state has a finite energy density above the ground state, and thus a large occupation of excited states, often described as quasiparticles states (QP). The subsequent dynamics can be described as the radiation of entangled pairs of QPs [14]. In translational invariant systems indeed QPs possess a well-defined dispersion relation $\epsilon(k)$, and a QP wave packet centered at k_0 propagates with group velocity $v_{k_0} = \partial_k \epsilon(k)|_{k_0}$, while momentum conservation enforces equal occupation of states that propagate with opposite momenta.

Identifying long-distance entanglement.—In order to identify the long-distance contributions to the entanglement we need to focus on a subsystem S of ℓ neighboring spins, and label L and R the remaining left and right regions of the

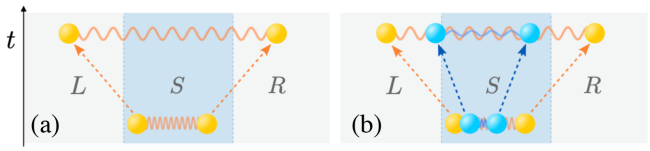

FIG. 1. (a) A correlated QP pair initially located inside region S creates long-distance (pure LR) entanglement when both QPs propagate outside of S. (b) At that time, slower QPs (blue) can still contribute to entanglement between S and its surroundings.

system (see Fig. 1). Entanglement across a bipartition (e.g., L vs SR) is created by correlated pairs of QPs with support on both sides of the cut. We define as *long-distance entanglement* the contribution to the entanglement generated by any QP pair supported on L and R, but not on S.

We can visualize this in the cartoon of Fig. 1(a), where we consider a quench that excites a single pair of entangled QPs, initially located inside S, that later travel with opposite velocities $\pm v$ [35]. In this simple example, S becomes entangled with the rest when one member of the pair leaves the region, but after $t \sim \ell/v$ both QPs have left, and the total state factorizes into the product of an entangled state of LR and a state of S.

In a more general scenario such complete factorization is not possible, since S and LR might contain other sources of entanglement. The simplest generalization depicted in Fig. 1(b) involves two pairs of QPs, one *fast* (orange) and one *slow* (blue). When the former has left S the latter is still partially in S. At that stage, it is still possible to disentangle a part of L and R from S. We can indeed identify a factorization of the Hilbert spaces, $L \equiv L_s \otimes L_f$ and $R \equiv R_s \otimes R_f$, such that the subsystem $L_f \otimes R_f$ is not entangled with S. In the simple scenario presented above, $L_f \otimes R_f$ is defined by the degrees of freedom that describe the fast pair, and we can factorize the state as $|\psi^{(\mathrm{slow})}_{L_s S R_s}\rangle \otimes |\phi^{(\mathrm{fast})}_{L_f R_f}\rangle$, where the second factor captures the pair of fast modes.

Trading long-distance entanglement for mixture.—In a translationally invariant system we can repeat the cartoon picture above for each block of ℓ sites. When computing the expectation value of a local observable, all the degrees of freedom are traced out, except those supporting the observable. For fast entangled pairs separated by at least ℓ sites, one partner will necessarily be traced out, leaving the other in a mixed state.

Thus, when focusing on local observables, we can describe the system as a mixed state where, for each fast pair, we have substituted the entangled state $\rho^{(\mathrm{fast})}_{L_f R_f}$ by $\tilde{\rho}^{(\mathrm{fast})}_{L_f R_f}$, the product of the mixed states obtained by tracing out each partner in the pair,

$$\rho^{(\mathrm{fast})}_{L_f R_f} = |\phi^{(\mathrm{fast})}_{L_f R_f}\rangle\langle\phi^{(\mathrm{fast})}_{L_f R_f}| \to \tilde{\rho}^{(\mathrm{fast})}_{L_f R_f} = \rho^{(\mathrm{fast})}_{L_f} \otimes \rho^{(\mathrm{fast})}_{R_f}, \quad (1)$$

where $\rho^{(\mathrm{fast})}_{L(R)} \equiv \mathrm{tr}_{R(L)}\left(\rho^{(\mathrm{fast})}_{LR}\right)$ are the reduced density matrices of each QP. This provides a more efficient local description in terms of entanglement, as the long-distance components have been removed.

From the QP intuition to a TN algorithm.—Standard MPS algorithms for this setup attempt to represent the time-evolved state as a MPS, parametrized by one or few tensors A_m of size $d \times D \times D$, where d is the physical dimension of the chain sites and D the bond dimension [39–41]. Since the half-chain entropy of the MPS is upper bounded by $\log D$ [4,42,43], the typical linear growth in time of entropy after a quench [14,16] requires an exponential increase of the tensor dimensions to maintain a constant precision. As a result, given finite computational resources, standard TN algorithms [44] only give reliable predictions for relatively short times (typically of the order $Jt \simeq 10$ with J the relevant energy scale).

Translating the QP intuition above to the TN setting we can however obtain a more efficient TN description for the local observables. Let us, for simplicity, assume that each MPS tensor represents precisely ℓ sites [45]. Singling out one subsystem, the whole state can thus be written as

$$|\Psi\rangle = \sum_{\alpha s_\ell \beta} C^{s_\ell}_{\alpha\beta} |\Phi^L_\alpha\rangle |s_\ell\rangle |\Phi^R_\beta\rangle, \quad (2)$$

where the sum is over orthonormal bases of the block and its left and right environments $\{|\Phi^{L/R}\rangle\}$, meaning that we use the gauge in which the tensor $C^{s_\ell}_{\alpha\beta}$ for the subsystem $\{|s\rangle\}$ is the orthogonality center of the MPS [13,39,46,47].

If there are long-range entangled degrees of freedom that decouple from S, the state will have a product structure, with one component completely disentangled from the physical degrees of freedom. There will thus exist basis transformations (disentanglers [48,49]) on L and R identifying the decomposition $L = L_f \otimes L_s$ and $R = R_f \otimes R_s$, such that

$$U^\dagger_L \otimes \mathbb{1}_S \otimes V^\dagger_R |\Psi\rangle = |\psi_{L_s S R_s}\rangle \otimes |\phi_{L_f R_f}\rangle, \quad (3)$$

as depicted in Fig. 2(I.a). If U_L and V_R exist, they can be determined minimizing the Euclidean distance between the left- and right-hand side of (3) [50]. Namely, given the evolved state in the form (2), and for fixed dimension d_{fast} of the long-range component, we iteratively optimize each of the disentanglers U_L and V_R and the vectors $|\psi_{L_s S R_s}\rangle$ and $|\phi_{L_f R_f}\rangle$ until the distance converges. Since the dimension d_{fast} of the fast factors L_f and R_f is unknown, the procedure needs to be repeated for different trial values.

Assuming the above procedure succeeds, we now can transform the identified long-range entanglement into mixture by applying the substitution (1) to each consecutive subsystem in the chain. As schematically shown in Fig. 2(I.b), this exchanges the pure MPS description of the system by a mixed

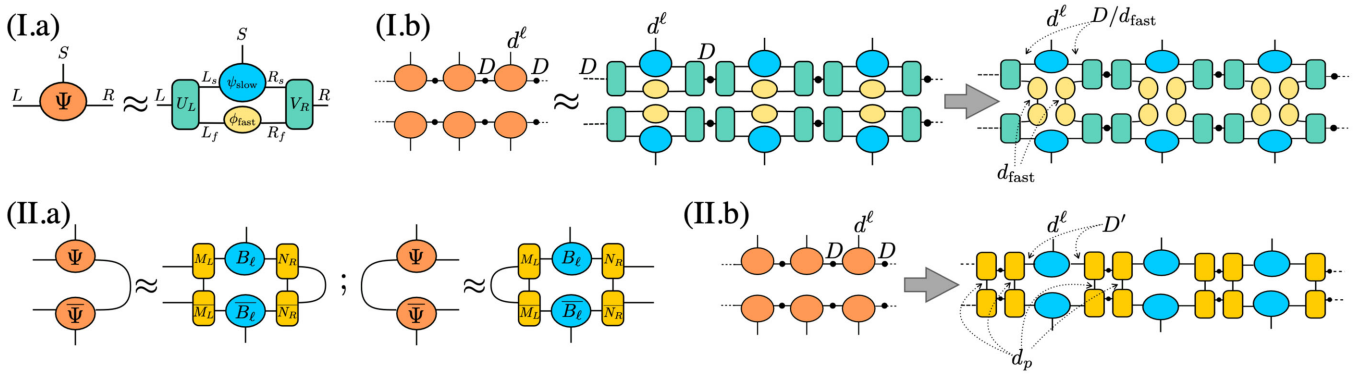

FIG. 2. First iteration in the transformation of long-range entanglement into mixture in TN. (I.a) Decomposition (3) for a block S, represented by a single tensor. (I.b) The density matrix of the full state (left) can be written in terms of the new tensors (middle) when we apply the decomposition to each block [black circles represent the inverse Schmidt values matrix, inserted to compensate for the central gauge in (I.a)]. We then substitute each long-range component by the product of its marginals, giving rise to a mixed description (right). (II.a) The heuristic algorithm directly searches for tensors that (approximately) preserve the reduced density matrices for LS and SR. (II.b) The density matrix for the full state is replaced by a purification defined by the solution. The structure is analogous to that in (I.b) (in each case we have indicated the relevant dimensions).

(purified) MPO with smaller bond dimension D/d_{fast}, at the expense of additional (purification) indices.

When the decomposition (3) is exact, this mixed state has the property that the reduced density matrices for $S_\ell R$ (respectively LS_ℓ) are unchanged [51]. As a consequence, also the reduced density matrix for two adjacent blocks, and thus all expectation values and correlation functions with support on up to ℓ sites are preserved. Larger supports can be achieved working with a larger ℓ, at the cost of longer disentangling times. We can then continue the evolution with the original Hamiltonian acting on the physical indices. Fast degrees of freedom will continue propagating entanglement through the subsystem S. Thus, the step of finding and mixing the long-range entangled components is repeated periodically.

An improved TN algorithm.—In practice, the best decomposition we identify using this strategy retains some residual entropy between fast and slow degrees of freedom $S(\rho_{\text{fast}})$. We apply the truncation when this entropy falls below a given threshold η_S. This results in small errors when building the mixed state that reflect in the evolution of local observables [see Fig. 4(a)]. Therefore we introduce an improved heuristic TN algorithm in which, after solving (3), if $S(\rho_{\text{fast}}) < \eta_S$ we propose an effective purification Ansatz, described by three rank-3 tensors, M_L, B_ℓ, and N_R, with fixed dimensions $d_p DD'$, $d^\ell D'^2$, and $d_p D'D$, where d_p is a chosen dimension for the purification index and $D' = D/d_p$ [see Fig. 2(c)].

The purification tensors are found variationally by minimizing the distance between the reduced density matrices ρ_{SR} (and ρ_{LS}) obtained from the original state (2) and from the purification. As initial guess we use the tensors obtained from solving (3), and we use gradient descent for the minimization problem (see [51]).

The dimension of the purification indices doubles after each mixing step. In practice, after few steps we keep it fixed by discarding the smallest eigenvalues of its reduced density matrix since we observe that the error induced by this truncation is negligible compared to other sources of errors in the simulation [52].

Numerical results.—We benchmark the algorithm using the transverse field Ising model with an additional integrability-breaking next-to-nearest-neighbor interaction,

$$H = -\sum_i (\sigma_i^z \sigma_{i+1}^z + g\sigma_i^x + J_2 \sigma_i^z \sigma_{i+2}^z). \tag{4}$$

Initially in a product state $|X+\rangle \equiv \otimes\, (1/\sqrt{2})(|0\rangle + |1\rangle)$, corresponding to the $g \to \infty$ ground state, the system is quenched to finite values of g, and potentially J_2.

To explore systematically the structure of the time-evolved MPS, we simulate accurately the short-time evolution using the infinite time-evolving block decimation (iTEBD) algorithm [39] with a large enough bond dimension. We then probe the disentangling of fast and slow degrees of freedom at different times solving (3) for a subsystem of $\ell = 2$ sites for several quenches.

As shown in Fig. 3, after a certain time we can identify subsystems of L and R that practically disentangle from the local region and carry long-range entanglement between the environments, measured by the logarithmic negativity [54,55] of the reduced density matrix for the fast degrees of freedom $\text{tr}_{L_s S R_s} |\Psi\rangle\langle\Psi|$. For all quenches, the residual entropy $S(\rho_{\text{fast}})$ decays fast with time, with a slower rate when quenching into the ordered phase [56]. As expected, the time at which fast degrees of freedom start decoupling from the local system depends linearly on ℓ [inset of Fig. 3(a)].

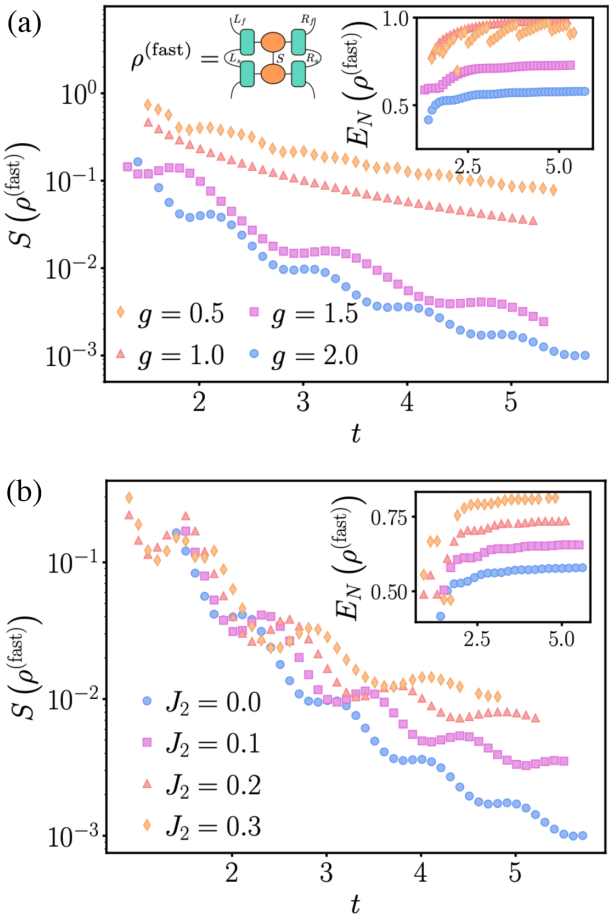

FIG. 3. Entropy (main plots) and left-right logarithmic negativity (insets) of the reduced density matrix for the *fast* degrees of freedom [see sketch in panel (a)], computed from the decomposition in Fig. 2(I.a) at different times (a) for several integrable quenches ($g \neq 0$, $J_2 = 0$) and (b) nonintegrable ones ($g = 2$, $J_2 \neq 0$).

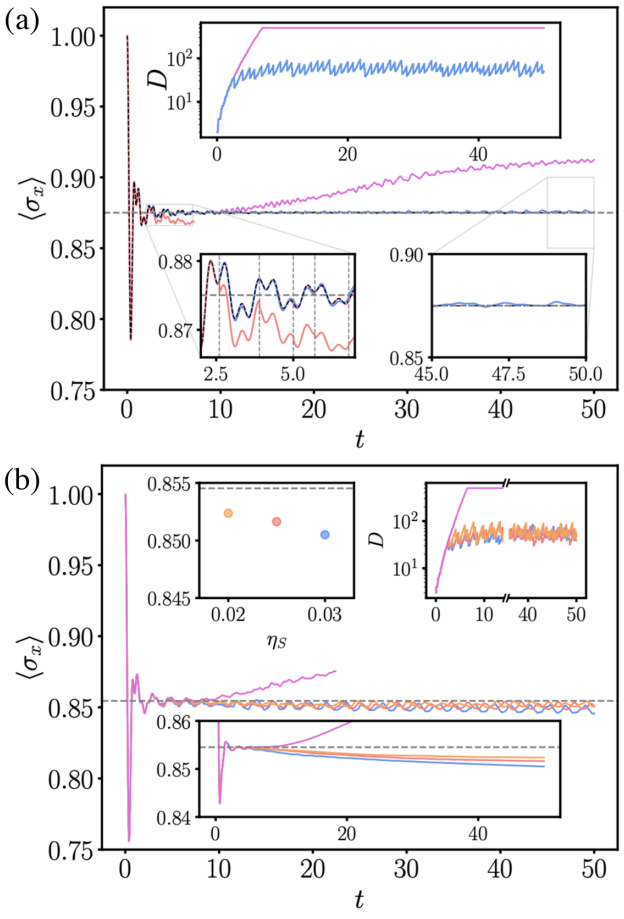

FIG. 4. (a) Evolution of the transverse magnetization for the integrable quench ($g = 2$, $J_2 = 0$) as obtained with the direct decomposition of Fig. 2(I) (orange) and the heuristic algorithm of Fig. 2(II) (blue). For comparison, we show the exact result (dashed black line), the equilibration value (dashed gray), and the iTEBD result with $D = 500$ (pink). The lower insets show enlargements of the short- and long-time regions. In the left one, the vertical dashed lines indicate mixing steps, inducing jumps in the simple but not the heuristic algorithm. (b) Same observable for the nonintegrable quench ($g = 2$, $J_2 = 0.1$) using the heuristic algorithm. Different colors indicate different residual entropy thresholds η_S. Our simulations converge toward the diagonal ensemble value $\langle\sigma_x\rangle_{\mathrm{DE}}$ (dashed gray line). This can be more clearly seen in the time average of the observable (lower inset) or the value of the time average at time $t = 50$ as a function of η_S (upper left inset). For both quenches, the upper (right) inset shows the bond dimension as a function of time.

We now use the TN algorithm described above and check its performance simulating the long-time evolution of local observables. Figure 4(b) shows the results for the integrable quench $g = 2$, $J_2 = 0$ and the only nonvanishing (due to the Z_2 symmetry) single-site observable $\langle\sigma_x\rangle$. Solving (3) and trading entanglement by mixture captures the qualitatively correct dynamics, but introduces discontinuous jumps (orange line and lower-left inset) that we attribute to the decomposition not being exact. The improved heuristic algorithm achieves much better results (blue line and lower-right inset). While the approximation induces some residual oscillations, these are very small, and the results are close to the exact equilibration even after considerably long times. In contrast, iTEBD results with a maximal bond dimension $D = 500$ (pink line) start to severely deviate from the exact solution at around $t = 10$.

Our algorithm uses instead a much smaller bond dimension: during the time evolution steps, the required bond dimension of the purified MPS grows exponentially, but each time we trade some of the entanglement for mixture, the bond dimension gets halved [57]. As we iterate the procedure, the maximum required bond dimension tends to a constant $D \sim 100$ (upper inset).

In Fig. 4(b) we repeat a similar analysis for the nonintegrable quench $g = 2$, $J_2 = 0.1$. The different colors show the results for different thresholds for the residual entropy η_S. Smaller values require longer evolution

between mixing steps, and thus larger bond dimension, but improve the results systematically.

Our results systematically approach the long-time limit predicted by the diagonal ensemble $\langle\sigma_x\rangle_{\mathrm{DE}} = 0.852$ [58].

Even for the largest threshold, the relative error in the time-averaged value after $t \sim 50$ is below 1% (0.848). Also the time-averaged magnetization exhibits a similar precision, as shown in the lower inset. Also in this case the largest bond dimension saturates with t (upper right inset).

In the Supplemental Material [51], we also repeat the calculations in the integrable case directly using the free-fermionic formalism [59] where we can track the coherence we discard in our simulation and confirm it does not play a relevant role in the long-time dynamics of local observables [51].

Discussion.—By identifying the long-range entanglement produced in the out-of-equilibrium dynamics after a quantum quench and converting it into mixture, we have proposed an explicit approach to avoid the entanglement barrier and simulate the out-of-equilibrium dynamics of an infinite quantum chain with MPS using finite computational resources.

Our approach is inspired by the intuitive understanding of entanglement dynamics in terms of the radiation of QP. It relies on the hypothesis that fast degrees of freedom propagate correlations to steadily growing distances, contributing to the linear growth of entanglement across the system, but only as a statistical mixture to sufficiently local observables. Our numerical results for the Ising chain show that the intuition is accurate in the free-fermionic case, which best fits the QP picture.

We have generalized our intuition to a heuristic algorithm that goes beyond the QP picture and also performs well in nonintegrable regimes of the model. It is thus important to pursue further characterization of the algorithm in order to chart its potential and limitations.

L. T. would like to thank Jacopo Surace who has contributed to developing the original ideas that have motivated this work. This work was partially supported by the Deutsche Forschungsgemeinschaft (DFG, German Research Foundation) under Germany's Excellence Strategy—EXC-2111–390814868; 499180199 and by the EU-QUANTERA project TNiSQ (BA 6059/1-1). L. T. acknowledges support from the Proyecto Sinérgico CAM 2020 Y2020/TCS-6545 (NanoQuCo-CM), the CSIC Research Platform on Quantum Technologies PTI-001 and from Spanish Projects No. PID2021-127968NB-I00 and No. TED2021-130552B-C22 funded by MCIN/AEI/FEDER, UE and MCIN/AEI/10.13039/501100011033, respectively.

*miguel.frias@mpq.mpg.de

[1] J. Eisert, M. Cramer, and M. B. Plenio, Rev. Mod. Phys. **82**, 277 (2010).
[2] J. I. Cirac, D. Pérez-García, N. Schuch, and F. Verstraete, Rev. Mod. Phys. **93**, 045003 (2021).
[3] F. Verstraete, V. Murg, and J. Cirac, Adv. Phys. **57**, 143 (2008).
[4] U. Schollwöck, Ann. Phys. (Amsterdam) **326**, 96 (2011), January 2011 Special Issue.
[5] R. Orús, Ann. Phys. (Amsterdam) **349**, 117 (2014).
[6] P. Silvi, F. Tschirsich, M. Gerster, J. Jünemann, D. Jaschke, M. Rizzi, and S. Montangero, SciPost Phys. Lect. Notes **46**, 8 (2019).
[7] S.-J. Ran, E. Tirrito, C. Peng, X. Chen, L. Tagliacozzo, G. Su, and M. Lewenstein, *Tensor Network Contractions*, Lecture Notes in Physics (Springer International Publishing, New York, 2020).
[8] K. Okunishi, T. Nishino, and H. Ueda, J. Phys. Soc. Jpn. **91**, 062001 (2022).
[9] M. C. Bañuls, Annu. Rev. Condens. Matter Phys. **14**, 173 (2023).
[10] M. Fannes, B. Nachtergaele, and R. F. Werner, Commun. Math. Phys. **144**, 443 (1992).
[11] S. R. White, Phys. Rev. Lett. **69**, 2863 (1992).
[12] S. Östlund and S. Rommer, Phys. Rev. Lett. **75**, 3537 (1995).
[13] D. Pérez-García, F. Verstraete, M. M. Wolf, and J. I. Cirac, Quantum Inf. Comput. **7**, 401 (2007).
[14] P. Calabrese and J. Cardy, J. Stat. Mech. 04 (2005) P04010.
[15] T. J. Osborne, Phys. Rev. Lett. **97**, 157202 (2006).
[16] N. Schuch, M. M. Wolf, K. G. H. Vollbrecht, and J. I. Cirac, New J. Phys. **10**, 033032 (2008).
[17] A. M. Läuchli and C. Kollath, J. Stat. Mech. 05 (2008) P05018.
[18] D. Rossini, S. Suzuki, G. Mussardo, G. E. Santoro, and A. Silva, Phys. Rev. B **82**, 144302 (2010).
[19] K. Van Acoleyen, M. Mariën, and F. Verstraete, Phys. Rev. Lett. **111**, 170501 (2013).
[20] M. C. Bañuls, M. B. Hastings, F. Verstraete, and J. I. Cirac, Phys. Rev. Lett. **102**, 240603 (2009).
[21] E. Leviatan, F. Pollmann, J. H. Bardarson, D. A. Huse, and E. Altman, arXiv:1702.08894.
[22] C. D. White, M. Zaletel, R. S. K. Mong, and G. Refael, Phys. Rev. B **97**, 035127 (2018).
[23] A. Hallam, J. G. Morley, and A. G. Green, Nat. Commun. **10**, 2708 (2019).
[24] C. Krumnow, J. Eisert, and Ö. Legeza, arXiv:1904.11999.
[25] L. Pastori, M. Heyl, and J. C. Budich, Phys. Rev. Res. **1**, 012007(R) (2019).
[26] J. Surace, M. Piani, and L. Tagliacozzo, Phys. Rev. B **99**, 235115 (2019).
[27] M. M. Rams and M. Zwolak, Phys. Rev. Lett. **124**, 137701 (2020).
[28] T. Rakovszky, C. W. von Keyserlingk, and F. Pollmann, Phys. Rev. B **105**, 075131 (2022).
[29] T. K. Kvorning, L. Herviou, and J. H. Bardarson, SciPost Phys. **13**, 080 (2022).
[30] M. Frías-Pérez and M. C. Bañuls, Phys. Rev. B **106**, 115117 (2022).
[31] M. Srednicki, Phys. Rev. E **50**, 888 (1994).
[32] C. Gogolin and J. Eisert, Rep. Prog. Phys. **79**, 056001 (2016).
[33] L. Vidmar and M. Rigol, J. Stat. Mech. 06 (2016) 064007.

[34] A. Mitra, Annu. Rev. Condens. Matter Phys. **9**, 245 (2018).
[35] This kind of simple dynamics is actually realized in a toy model of local unitaries [20,36] and in some concrete physical realizations such as the split quenches studied in [37,38].
[36] A. Müller-Hermes, J. I. Cirac, and M. C. Bañuls, New J. Phys. **14**, 075003 (2012).
[37] A. Zamora, J. Rodríguez-Laguna, M. Lewenstein, and L. Tagliacozzo, J. Stat. Mech. 09 (2014) P09035.
[38] Y. Chen and G. Vidal, J. Stat. Mech. 10 (2014) P10011.
[39] G. Vidal, Phys. Rev. Lett. **98**, 070201 (2007).
[40] J. Haegeman, J. I. Cirac, T. J. Osborne, I. Pižorn, H. Verschelde, and F. Verstraete, Phys. Rev. Lett. **107**, 070601 (2011).
[41] L. Vanderstraeten, J. Haegeman, and F. Verstraete, SciPost Phys. Lect. Notes, 7 (2019).
[42] D. Perez-Garcia, F. Verstraete, M. M. Wolf, and J. I. Cirac, Quantum Inf. Comput. **7**, 401 (2007).
[43] G. Evenbly and G. Vidal, J. Stat. Phys. **145**, 891 (2011).
[44] S. Paeckel, T. Köhler, A. Swoboda, S. R. Manmana, U. Schollwöck, and C. Hubig, Ann. Phys. (Amsterdam) **411**, 167998 (2019).
[45] This can always be obtained by blocking together ℓ tensors of the original systems to yield a single tensor.
[46] L. Vanderstraeten, J. Haegeman, and F. Verstraete, SciPost Phys. Lect. Notes 7 (2019).
[47] G. Evenbly, arXiv:2202.02138.
[48] G. Vidal, Phys. Rev. Lett. **99**, 220405 (2007).
[49] G. Evenbly and G. Vidal, Phys. Rev. B **79**, 144108 (2009).
[50] T. Kraft, C. Ritz, N. Brunner, M. Huber, and O. Gühne, Phys. Rev. Lett. **120**, 060502 (2018).
[51] See Supplemental Material at http://link.aps.org/supplemental/10.1103/PhysRevLett.132.100402 for more details.
[52] Other schemes would be possible to try and optimize the purification sites, for instance, in the spirit of the optimal purification of [53].
[53] J. Hauschild, E. Leviatan, J. H. Bardarson, E. Altman, M. P. Zaletel, and F. Pollmann, Phys. Rev. B **98**, 235163 (2018).
[54] G. Vidal and R. F. Werner, Phys. Rev. A **65**, 032314 (2002).
[55] M. B. Plenio, Phys. Rev. Lett. **95**, 090503 (2005).
[56] This is consistent with the distribution of momentum excitations in the initial state, computed in the exact free-fermionic formulation, which is peaked at finite velocities when the quench is within the same phase, and at zero velocity otherwise (see the Supplemental Material [51]).
[57] We use $d_p = 2$ for our Ansatz.
[58] Extrapolated from exact finite size results.
[59] J. Surace and L. Tagliacozzo, SciPost Phys. Lect. Notes 54 (2022).